Supplementary Information

Supplementary Table 1. Summary of subject information and the feeding behavior test

	Sex	Age (y)	Observed number			Test duration (s)
			floor-hand	floor-head	wall	
Marmo1	F	2.7	10	5	4	340
Marmo2	F	1.4	5	2	3	200
Marmo3	M	6.4	9	3	3	220
Marmo4	M	5.1	7	5	3	260

Supplementary Table 2: Proportion of variance explained by the top five principal components extracted from the marmoset free-feeding behavior

	PC1	PC2	PC3	PC4	PC5
Standard deviation	2.45	1.71	1.24	0.75	0.69
Variance explained	0.46	0.23	0.12	0.04	0.04
Cumulative proportion	0.46	0.69	0.80	0.85	0.88

Supplementary Table 3: Distribution of observed motion motifs for each individual marmoset

	Motion unit																	
	1	2	3	4	5	6	7	8	9	10	11	12	13	14	15	16	17	18
Marmo1	3	4	8	0	4	5	6	1	2	2	3	2	1	4	5	5	2	7
Marmo2	10	5	6	3	7	8	10	6	3	0	7	5	6	4	2	1	3	1
Marmo3	6	5	6	4	3	8	7	2	0	4	1	1	3	1	6	3	2	5
Marmo4	1	8	7	1	9	6	12	3	3	2	5	6	1	7	8	8	0	7

Supplementary Table 4. Distribution of posture clusters at feeding timing using the posture model (k = 18)

	Posture cluster																	
Feeding subtype	1	2	3	4	5	6	7	8	9	10	11	12	13	14	15	16	17	18
wall	13	1	1	0	0	0	0	0	4	24	1	3	1	13	1	1	0	0
floor-head	8	1	1	0	0	0	0	0	4	15	0	3	1	8	1	1	0	0
floor-hand	5	0	0	0	0	0	0	0	0	9	1	0	0	5	0	0	0	0

Supplementary Table 5: Proportion of variance explained by the top five principal components extracted from the monkey free-motion behavior

OpenMonkeyPose	PC1	PC2	PC3	PC4	PC5
Standard deviation	3.48	2.10	1.82	1.52	1.38
Variance explained	0.34	0.12	0.09	0.06	0.05
Cumulative proportion	0.34	0.46	0.55	0.62	0.67

Supplementary Table 6: Proportion of variance explained by the top five principal components from the marmoset neural manipulation analysis

	PC1	PC2	PC3	PC4	PC5
Standard deviation	2.75	2.21	1.97	1.42	1.19
Variance explained	0.29	0.19	0.15	0.08	0.05
Cumulative proportion	0.29	0.48	0.63	0.73	0.81

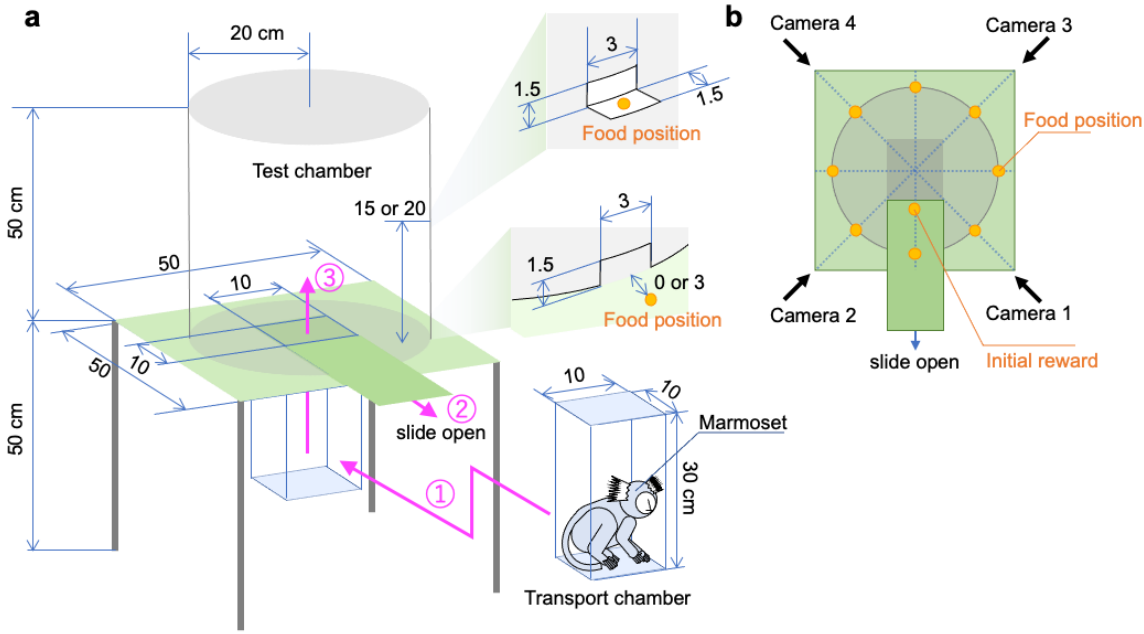

Supplementary Figure 1 Experimental setup

(a) Animals entered the behavior test chamber from the transport chamber by opening the door at the bottom of the test chamber floor. They then freely ate the food set in the small windows on the floor and the wall. A piece of food was placed at the entrance to guide the animals into the test chamber. **(b)** Four depth cameras were placed at 45-degree intervals to record three-dimensional behavior.

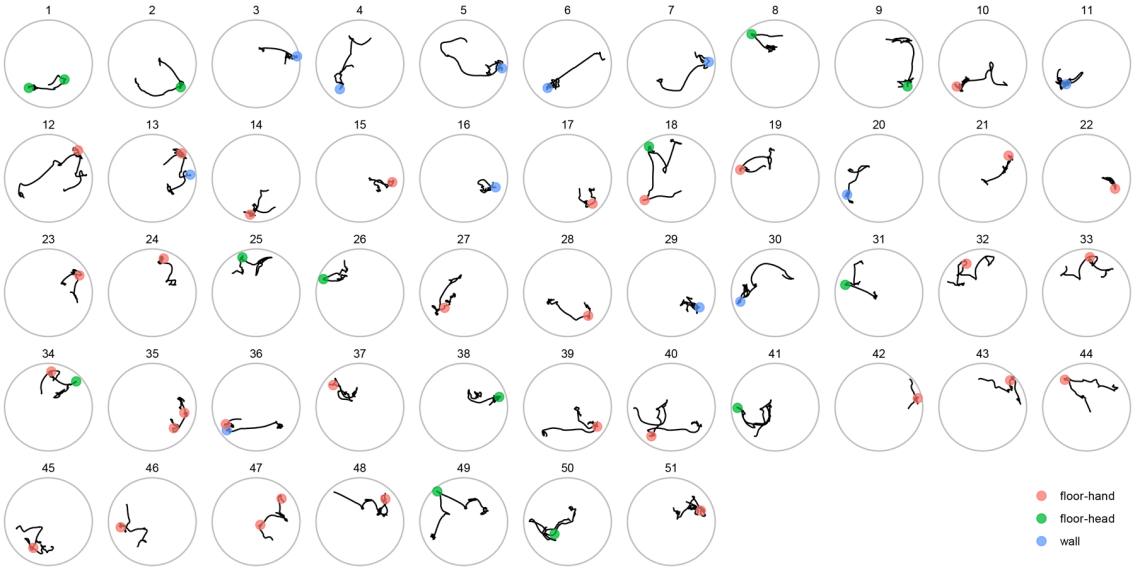

Supplementary Figure 2 *Head* trajectories of marmoset free-feedings

Top view of marmoset *Head* trajectory during free-feeding behavior used in the SMP analysis. The data include 51 segments of 20-s behaviors (a total of 993 s). The trajectories were synthesized from video recorded by four depth cameras. Colored dots indicate the locations and types of feeding (red, floor-hand; green, floor-head, and wall, blue). The gray circles indicate the cylinder wall (50 cm radius).

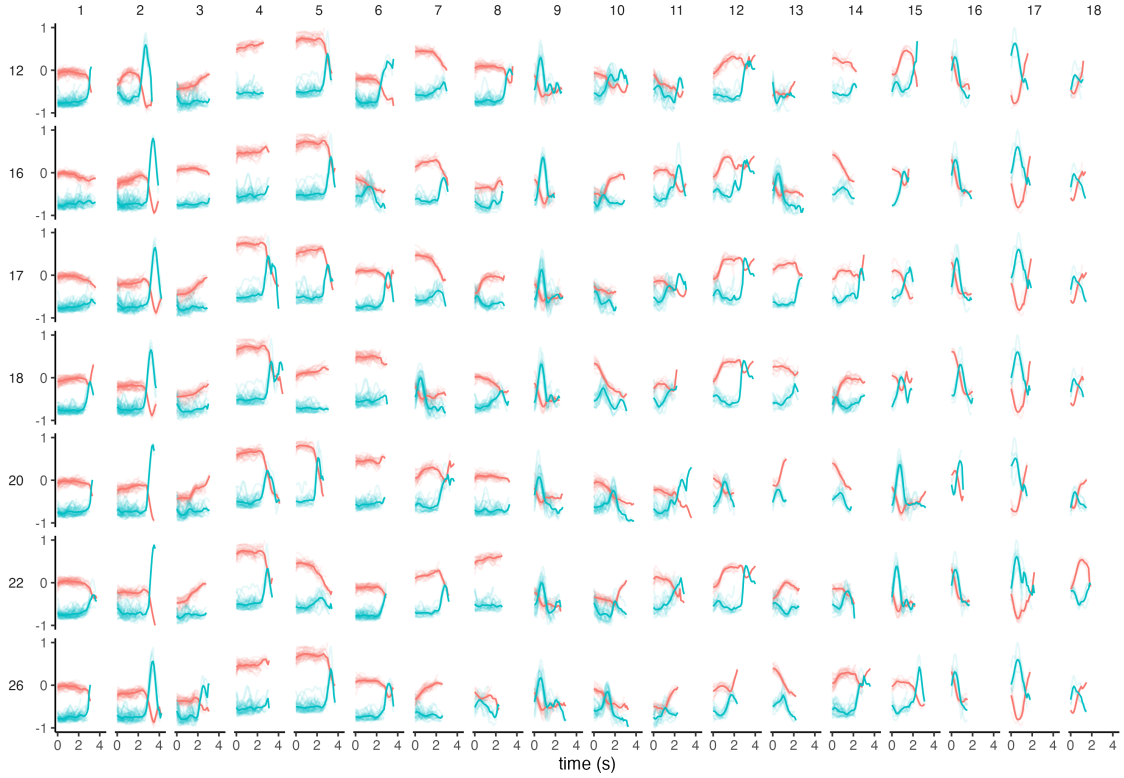

Supplementary Figure 3 Consistency of SMP classification of marmoset free-feeding behaviors

Temporal dynamics of principal component scores (PC1, red; PC2, green) for 18 motifs (1 to 18 at top) are shown as the results of simulations with different initial class sizes (from 12 to 26 in left). The second to last row (initial class size = 22) corresponds to the results shown in Fig. 2h.

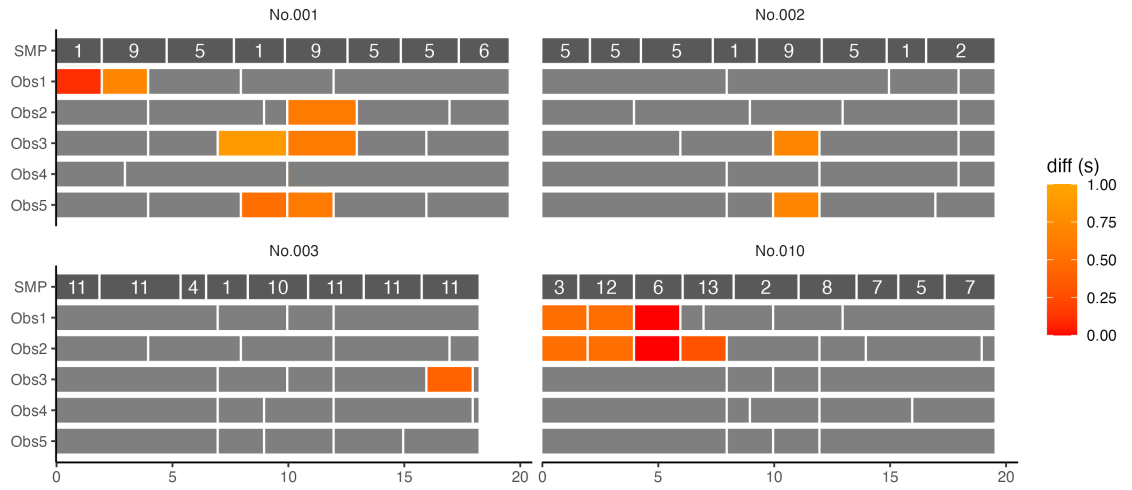

Supplementary Figure 4 Comparison of SMP motifs and manual expert-segmented motifs extracted from marmoset feeding behavior

The graphs illustrate the results of SMP and expert manual segmentation for four feeding-behavior sequences (corresponding to 1, 2, 3, and 10 shown in Supplementary Fig. 2). For each panel, the upper row (SMP) displays the output of SMP labeled with motif numbers that correspond to those in Supplementary Figure 3. The lower five rows (Obs1-5) represent the results of segmentation by five expert observers. The manual segments that closely aligned with SMP motifs are colored according to the sum of the differences at start and end points.

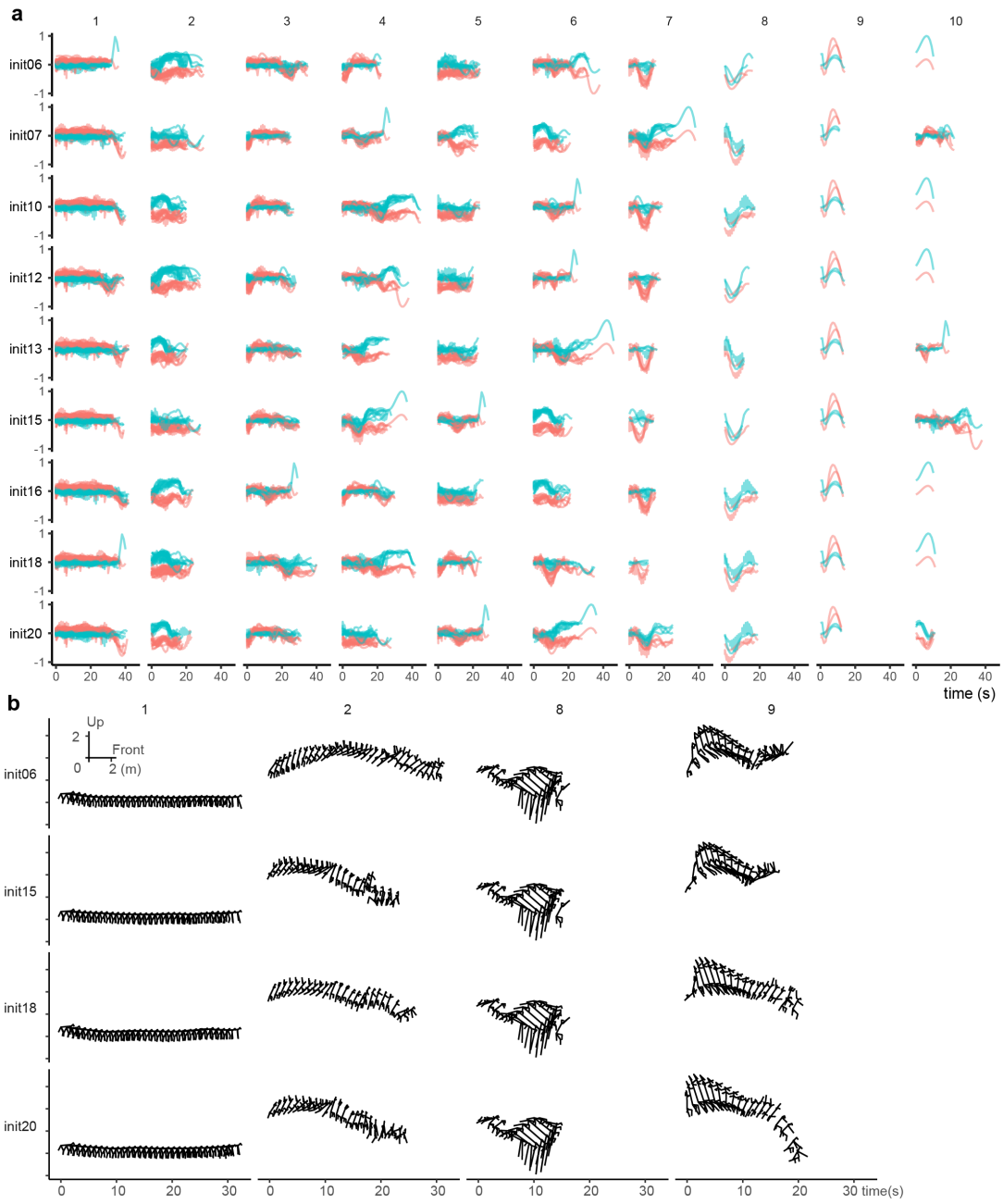

Supplementary Figure 5 Consistency of SMP classification of macaque free-moving behavior

(**a**) Temporal dynamics of principal component scores (PC1, red; PC2, green) for 10 motifs (1 to 10 at top) are shown as the results of simulations with different initial class sizes (from 6 to 20 in left). **(b)** The synthesized ideal body trajectories estimated by inverting the PCs corresponding to motifs 1, 2, 8, and 9, with four different initial class size.

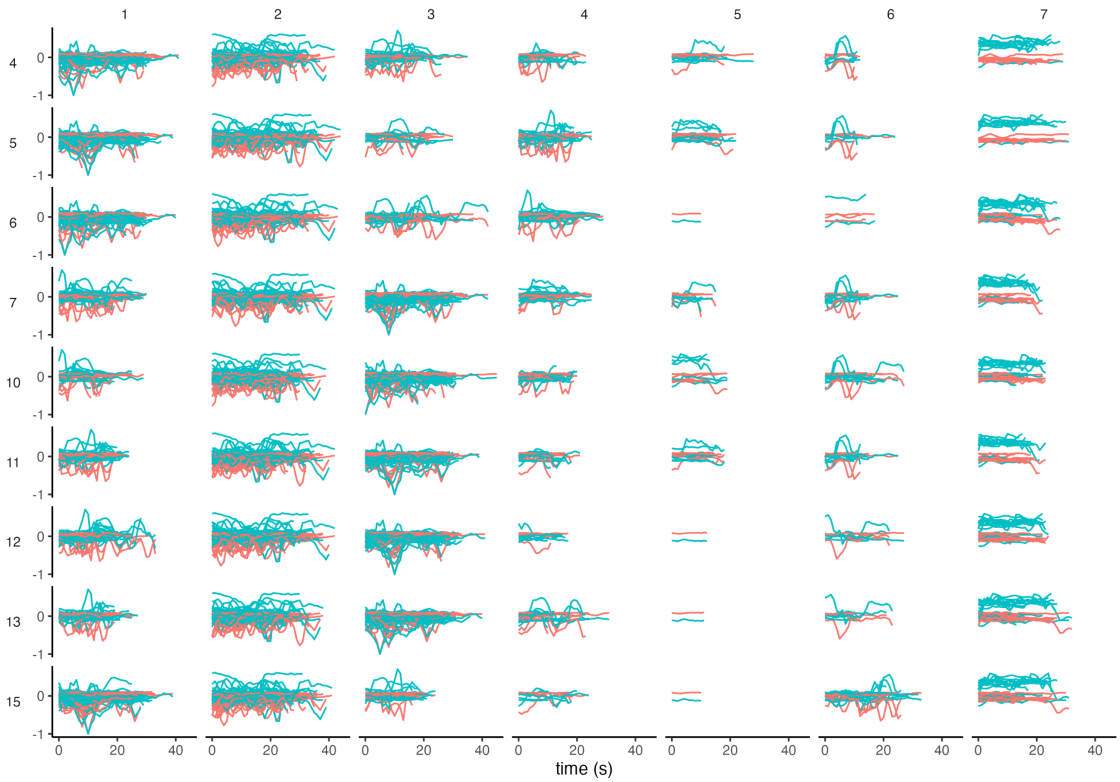

Supplementary Figure 6 Consistency of SMP classification of marmoset behavior induced by neural manipulation

Temporal dynamics of principal component scores (PC1, red; PC2, green) for 7 motifs (1 to 7 at top) are shown as the results of simulations with different initial class sizes (from 4 to 15 in left).

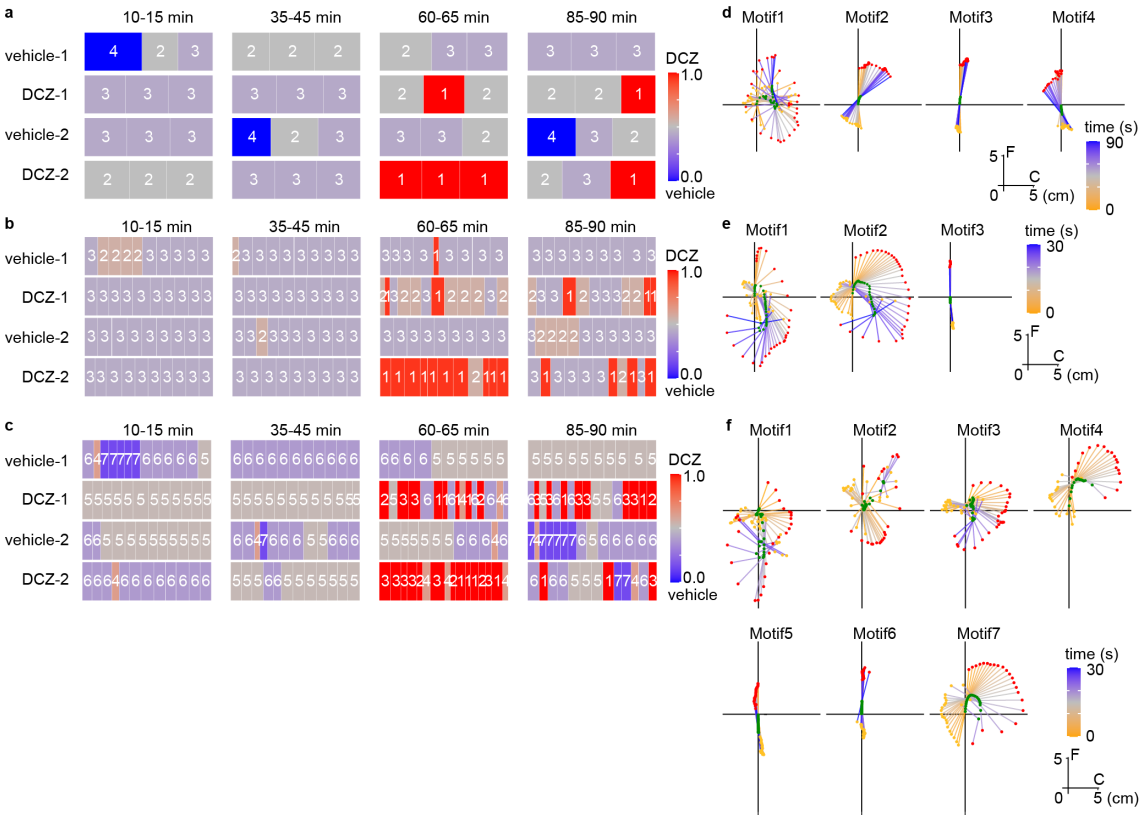

Supplementary Figure 7 Effects of hyperparameters

(a-c) Effect of changing SMP parameters on the sequence of motion motifs extracted from marmoset rotation behavior induced by chemogenetic neuronal manipulation. (a) The initial motif length is set to the mean of 90 s (min 75 s, max 150 s). (b and c) The first principal component score (PC1) and three PCs (PC1 to PC3) are used without changing the motif length (mean 30 s, min 10 s, max 70 s). Compared with the results using the two PCs shown in Fig. 5f, using only one PC significantly reduced the richness of data interpretation, while increasing to three PCs provided minimal additional insight, while increasing computational demands. **(d-f)** The top view of the body trajectories of SMP motion motifs estimated by inverting the PCs corresponding to **a**, **b**, **c** respectively. See also Fig. 5f-g.

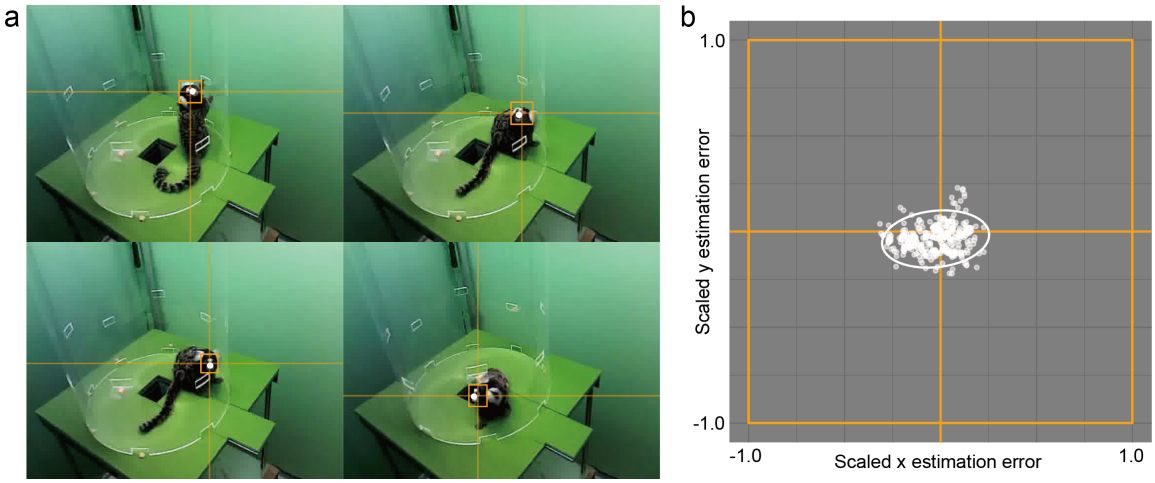

Supplementary Figure 8 Estimation error of marmoset Face direction

(a) Examples of 2D projection images of the *Face* position (orange rectangle with x and y axes) estimated by YOLO3 and those that were manually annotated (white point). **(b)** Scatter and density-error plots between manual annotation and estimated results and 95% confidence ellipse on 2D images calibrated with the orange *Face* rectangle sizes in 350 randomly selected frames. Mean ± SEM errors for the frame were -0.026 ± 0.0066 and -0.037 ± 0.0039, on the X- and Y- axes, respectively.